

Non-reciprocal alignment induces asymmetric clustering in active repulsive mixtures

Kim L. Kreienkamp* and Sabine H. L. Klapp†

Institut für Theoretische Physik, Technische Universität Berlin

Heterogeneity is a ubiquitous feature in many biological and synthetic active matter systems that are inherently out of equilibrium. In addition to conservative interactions between active constituents, a non-equilibrium environment often induces effective non-reciprocal (NR) couplings. The full consequences, especially for systems with order parameters of different symmetries, still remain elusive. Here, we study a minimal active NR mixture exhibiting both, polar ordering and clustering using a combination of hydrodynamic theory, linear stability analysis, particle-based simulations and fluctuation analysis. We show that NR alignment interactions have profound influence on the density dynamics already far below the threshold related to spontaneous time dependency of polarization dynamics. In particular, NR alignment alone induces *asymmetrical* clustering, and thus, partial demixing with single-species clusters chasing more dilute accumulations of the other species. Extremely large NR alignment eventually leads to a disappearance of clustered states.

The phase behavior of fluid mixtures and, in particular, their spontaneous demixing, is a topic fascinating researchers for decades [1]. In thermal equilibrium, the basic mechanisms are well understood in terms of (effective) interactions and entropy: demixing occurs, e.g., when particles differ in shape [2] or size [3, 4], or if interactions between different species are weak against the attraction within species [5]. The situation becomes more complex in living and active systems that are inherently out of equilibrium and, at the same time, often heterogeneous: examples range from bacterial colonies and heterogeneous bacterial swarms [6–8] to synthetic active-passive mixtures [9, 10] and multicomponent biological membranes [11, 12]. Therefore, and since already one-component active systems exhibit intriguing self-organization such as flocking [13–15], motility-induced phase separation (MIPS) [16, 17] and clustering [18], the dynamical phases of active *mixtures* (with, e.g., differing motilities [19–21], diffusivities [22], or shapes [8, 23]) are currently receiving strong interest. However, we are still far away from a comprehensive understanding of self-organization in active mixtures. Here we address, in particular, the role of nonreciprocal (NR) couplings.

On the microscale, *effective* NR couplings are typically induced by a non-equilibrium environment [24, 25], that occurs, e.g., for phoretic colloids [26–29], hydrodynamically interacting colloids [23, 25, 30], or in quorum sensing [14, 31, 32]. More generally, NR plays an important role in macroscopic predator-prey systems [33–35], systems with vision cones [36–39], odd solids [24, 40], and quantum optics [41–43]. Recent field-theoretical studies [44–49] and particle-based simulations [31, 50] have shown that NR couplings alone have indeed drastic effects, including the spontaneous formation of time-dependent (traveling or chiral) states [44–46]. So far, the density dynamics of scalar NR mixtures, on the one hand, and orientational dynamics of polar NR mixtures, on the other hand, have been discussed quite separately. Therefore, the dynamics of NR mixtures involving several types of order parameters with different symmetries (and poten-

tially different conservation rules) remains, so far, elusive, although such order-parameter coupling is indeed quite common [51]. Recent experiments [23] have already indicated unexpected phase separation in mixtures of hydrodynamically interacting Quincke rollers [52] where aligning torques couple to positions. In this Letter we ask, on a theoretical basis, the question: How do NR polar couplings *alone* affect systems featuring clustering and MIPS? Can such NR alignment even induce demixing?

To this end we consider a minimal model of a binary mixture of spherical ABPs with fully symmetric repulsive interactions (favoring MIPS) and reciprocal intraspecies alignment interactions (favoring flocking within each species). The NR character enters only via the interspecies alignment which may be asymmetric and even antagonistic (i.e., of opposite sign). Importantly, the orientational interactions are unrelated to the spatial configuration (different to, e.g., hydrodynamic or dipolar interactions). Without repulsion, our model reduces to a polar NR mixture of point-like particles exhibiting spontaneous chiral motion of the polar director at large coupling strengths [45]. Here, in order to focus on the density dynamics, we operate in a “weak-coupling” regime, in which flocking interferes with MIPS and becomes suppressed for strong enough non-reciprocity. Based on a mean-field (MF) hydrodynamic theory and linear stability analysis we present a full non-equilibrium phase diagram. In addition, we perform particle-based simulations and a corresponding fluctuation analysis to unravel effects beyond MF theory. Intriguingly, we find that NR orientational interactions, that are *not* coupled to positional configuration, can suppress MIPS. Moreover, for a broad range of parameters, we observe asymmetric density dynamics manifested by the formation of clusters of only *one* species, akin to partial demixing. While this effect is predicted already by the linear stability analysis, only particle-level calculations reveal the single-species cluster dynamics characterized by chase-and-run behavior and strong polarization.

Model.—We consider a two-component mixture of

spherical ABPs with equal densities $\rho_0^a = \rho/2$ ($a = A, B$), equal self-propulsion velocities, equal translational and rotational noises, and fully symmetric repulsive interactions [SM]. The direction of the heading vectors $\mathbf{p}_a = (\cos \theta_a, \sin \theta_a)^T$ is subject to random noise and a torque given by $T^a \propto \sum_b g_{ab} \sin(\theta_a - \theta_b)$. We set the intraspecies alignment couplings equal, i.e., $g_{AA} = g_{BB} = g$, whereas the interspecies values g_{AB} , g_{BA} can be non-symmetric, yielding NR. For the detailed equations of motion and corresponding Brownian Dynamics (BD) simulations, see [SM]. Coarse-graining the microscopic dynamics in mean-field (MF) approximation (and incorporating a density-dependent velocity) [45, 53, 54] [SM], we then obtain a hydrodynamic description of the spatio-temporal dynamics of the (conserved) density fields $\rho^a(\mathbf{r}, t)$ and (non-conserved) polarization densities $\mathbf{w}^a(\mathbf{r}, t)$, yielding equations of the form $\partial_t \rho^a = -\nabla \cdot \mathbf{j}(\mathbf{w}^a, \rho^{a,b}, \nabla \rho^a)$ and $\partial_t \mathbf{w}^a = F(\mathbf{w}^{a,b}, \rho^{a,b}, \nabla^2 \rho^{a,b}, \nabla^2 \mathbf{w}^{a,b}, \nabla \rho^{a,b}, \nabla \mathbf{w}^{a,b}, \dots)$.

Emergent phase behavior.—Henceforth, we choose the density, motility, and noise strengths such that, in the absence of polar couplings ($g_{ab} = 0$), the system exhibits MIPS. The (non-dimensionalized) intraspecies alignment coupling strengths g_{aa} are set to $g_{aa} = g = 3$. In the resulting effective one-species system $g_{ab} = g$ ($\forall ab$) a phase-separated flocking state emerges, characterized by the formation of a dense, mixed-species cluster with large overall polarization. To elucidate the dynamical behavior upon varying, independently, g_{AB} and g_{BA} , we first perform a stability analysis of the hydrodynamic equations around the homogeneous isotropic state as functions of the wavenumber, k , of perturbations. Analyzing the resulting six-dimensional stability matrix we obtain the stability diagrams given in Fig. 1 [SM]. At $k = 0$ [Fig. 1(a)], all instabilities are related to long-wavelength fluctuations of the polarizations [53], leading to (anti-)flocking states with global polarization order parameter $P_a = |\mathbf{P}_a| = |N_a^{-1} \sum_{\alpha}^N \mathbf{p}_\alpha| > 0$ at sufficiently strong interspecies coupling. Unstable density dynamics comes into play at $k > 0$, see full diagram in (b). A detailed structural analysis and comparison with nonlinear continuum simulations are provided in [55].

We first consider the reciprocal line defined by $g_{AB} = g_{BA} = \kappa$. Starting from the effective one-component system ($g = 3$), an increase of κ enhances the flocking behavior, comparable with an increase of the overall alignment coupling. In turn, a decrease of κ towards values smaller than g first yields a disappearance of polar order, since the relative strength of polar coupling becomes too small. This results in pure phase separation. Orientational order is recovered for negative values of κ , where the two species each form flocks, yet with antiparallel direction [anti-flocking, see Fig. 1(c)]. These stability results for reciprocal systems are qualitatively consistent with those from BD simulations, see marker points in Fig. 1(b). Moving away from the reciprocal line changes

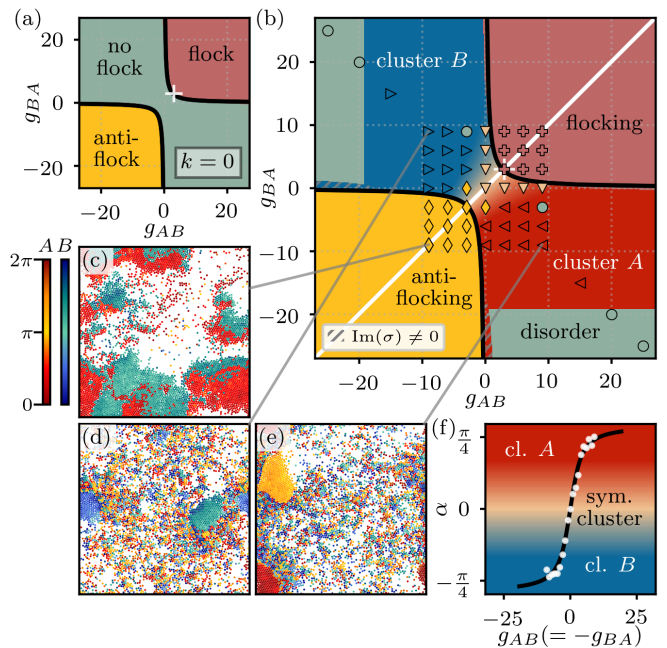


FIG. 1. Nonequilibrium phase behavior at weak coupling ($g = 3$). (a) MF stability diagram at $k = 0$. (b) Full MF stability diagram (including $k > 0$), revealing regions of asymmetric clustering and disorder. Color-coded marker points denote corresponding BD simulations. The white cross in (a,b) indicates the effective one-component system. (c-e): BD snapshots for (c) $g_{AB} = g_{BA} = -9$, (d) $g_{AB} = -g_{BA} = -9$, and (e) $g_{AB} = -g_{BA} = 9$. Color code indicating particle type and orientation is provided in (c). (f) MF predictions (line) and BD data (dots) for the angle α characterizing asymmetric clustering.

the dynamical behavior drastically, particularly in the antagonistic regions where the signs of g_{AB} , g_{BA} are opposite. We start from the point $g_{AB} = g_{BA} = 0$ and move on the line $g_{AB} = \delta = -g_{BA}$ into the fully antisymmetric regime. The symmetric phase separated state, characterized by mixed clusters, then transforms into a state characterized by *asymmetric* density dynamics. Here, as signaled by the stability analysis [SM] and directly observable in BD simulations [see Fig. 1(d,e)], clusters of *only one* species form whose type (A or B) depends on the sign of δ . In other words, we observe a partial demixing induced by NR orientational coupling between different species. The clusters themselves are polarized, that is, $P_{\text{cluster}} \gtrsim 0.7$. The partial demixing is unexpected in view of the fully symmetric steric interactions (and the symmetry of g_{aa}). Indeed, in our model any coupling asymmetry arises only through the interspecies torques that, however, do not couple to the particle positions. The observed phenomenon is robust against variation of initial conditions. Moreover, simulation movies [SM] in this regime reveal “chasing” behaviors familiar from other NR off-lattice systems [26, 44, 46, 50, 56]. Eventually, for very strong NR ($|\delta| \gtrsim 20$), clustering is fully

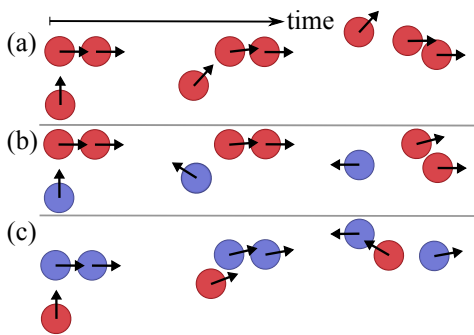


FIG. 2. Schematic of particle motion eventually leading to asymmetric clustering of species A ($g = 3$, $\delta = 9$). Particles of species A (B) are colored in red (blue). Starting from a “cluster” of two coherently moving particles of same species, (a)-(c) depict the clusters’ time evolution upon approach of a third particle. A -clusters survive (a,b) whereas B -clusters are destabilized (c).

suppressed, yielding a homogeneous disordered state.

Microscopic origin of asymmetric clustering.—To unravel the origin of the asymmetric clustering, we consider, as an example, the case $\delta = 9$, $g = 3$, such that A tends to orient along B (and A) while B wants to orient opposite to A (and along B). Particles of species A therefore have overall a higher tendency to align with other particles. In Fig. 2 we illustrate the evolution of a small “cluster” involving two coherently moving A - or B -particles upon approach of another particle. If the approaching particle is from the same species [case (a)] it either joins the cluster; or at least, does not significantly disturb the cluster’s motion. If a B -particle approaches an A -cluster [case (b)], it quickly reorients into the opposite direction (since $g_{BA} < 0$) and thereby tends to move away. Thus, B does not join the A -cluster, but also does not disturb it. In contrast, if an A -particle approaches a B -cluster (c), it tends to orient along the cluster’s direction ($g_{AB} > 0$). However, this disturbs the coherent motion of the B -particles, since the latter now tend to orient opposite to A (recall that the intraspecies coupling is relatively weak). As a consequence, the B -cluster is destabilized.

Fluctuation analysis.—The asymmetric clustering is also reflected by two-particle correlation functions. In Fig. 3 we plot the functions $G_{ab}(r)$ [SM] measuring the angle-averaged distribution of a -particles around a particle of species b at distance r (for corresponding orientational correlations, see [55]). The data are obtained shortly after initialization from a disordered configuration. In the reciprocal case, we always find $G_{AA} = G_{BB}$, while G_{AB} may be smaller or larger depending on the ratio g/κ . In contrast, the asymmetrically clustered state is characterized by $G_{AA} \neq G_{BB}$. In particular, at the parameters of Fig. 2, $G_{AA} > G_{BB}$, indicating the preference of A -clustering.

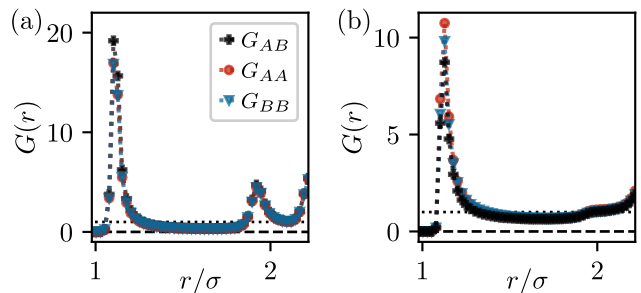


FIG. 3. Pair correlation functions for (a) $g_{AB} = g_{BA} = 9$, (b) $g_{AB} = \delta = -g_{BA} = 9$ (and $g = 3$). Data represent time averages between 0.5 and 1τ after initialization.

Given the information contained in the short-time correlations, we now use these for a systematic analysis of fluctuations (similar to equilibrium stability analysis of phase transitions in binary mixtures [57–59]). This provides an alternative way to check the system’s stability beyond MF theory. Here we concentrate on long-wavelength fluctuations of the total density, $\delta\hat{\rho}(k) = \delta\hat{\rho}_A(k) + \delta\hat{\rho}_B(k)$, the concentration $\delta\hat{c}(k) = \delta\hat{\rho}_A(k) - \delta\hat{\rho}_B(k)$, and mixtures of these [57, 58]. Their magnitude is given by the structure factors $S_{ij}(k) = \langle \delta\hat{i}(k)\delta\hat{j}(k) \rangle$ ($i, j = \rho, c$) that can be computed as Fourier transforms of corresponding $G_{ab}(r)$ [57, 58][SM]. If the homogeneous system becomes unstable, one expects one or several elements of the symmetric 2×2 matrix \mathcal{S} with elements $S_{ij}(k)$ to diverge. For a systematic analysis we diagonalize \mathcal{S} , focusing on the limit $k \rightarrow 0$ (which turns out to be most relevant). An instability is signalled by divergence of one eigenvalue $\lambda_{1/2}$ of \mathcal{S} , or equivalently, a vanishing of its inverse, $\lambda_{1/2}^{-1}$. We assume that the direction of the corresponding eigenvector in the $\delta\hat{\rho}-\delta\hat{c}$ -plane, quantified by the angle α , indicates the dominant character of the instability. Symmetric clustering or full, symmetric demixing correspond to $\alpha = 0$ and $\alpha = \pm\pi/2$, respectively. Further, $0 < \alpha < \pi/2$ ($-\pi/2 < \alpha < 0$) indicate asymmetric clustering of species A (B).

Results are shown in Fig. 4. In the reciprocal case $g_{AB} = g_{BA} = 0$ (a), the fluctuation analysis predicts a symmetric clustering instability with $\lambda_1^{-1} \approx 0$ and $\alpha \approx 0$, consistent with the observation of MIPS in Fig. 1. Moving into the fully antisymmetric regime (i.e., increasing $|\delta|$ from zero), $\lambda_{1/2}^{-1}$ become non-zero indicating that the density fluctuations are strong, yet not divergent any more. At the same time, α continuously changes, now indicating asymmetric clustering. Setting $g_{BA} = -9$ constant [Fig. 4(b)], and increasing g_{AB} from -9 to 9 implies that we move along a horizontal path from reciprocal antiflocking towards the NR A -clustering regime [see Fig. 1(b)]. At the beginning, the $\lambda_{1/2}^{-1}$ are close to zero. Together with $\alpha \approx \pm\pi/2$ this means that the reciprocal antiflocking state is indeed associated to a demixing instability, an observation which conforms with the vi-

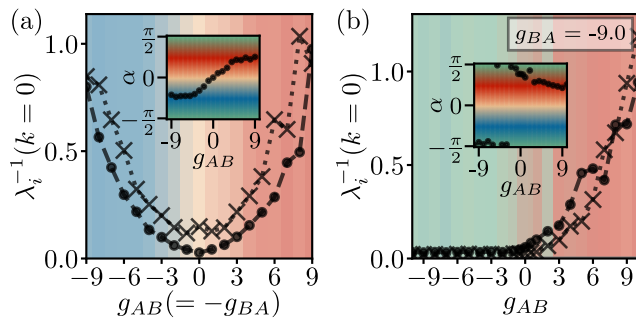


FIG. 4. (Inverse) eigenvalues $\lambda_{1/2}^{-1}$ of $\mathcal{S}(k \rightarrow 0)$ and predicted angle α (inset) from BD simulations. (a) $g_{AB} = \delta = -g_{BA}$. (b) $g_{BA} = -9$ (and $g = 3$). Data represent time averages between 4.5 and 5τ after the start of the simulation.

sual inspection [Fig. 1(c)]. At larger g_{AB} , asymmetric A-clustering becomes more and more dominant, consistent with the results of the MF analysis. Indeed, the agreement between the stability analysis on different level of descriptions (BD simulations versus MF hydrodynamics) holds not only from a qualitative point of view, but also *quantitatively*. This is seen in Fig. 1(f) where we directly compare, for a given path in the state diagram, the angles α from the two types of calculations. Moreover, both methods indicate that the transformation from reciprocal MIPS to asymmetric clustering is gradual.

Towards larger coupling strengths.—All of the above results have been obtained at relatively weak g_{aa} , where non-reciprocity can suppress flocking. Within the MF stability analysis, the largest eigenvalues characterizing the dominant unstable fluctuations are *real-valued* essentially everywhere in Fig. 1 [60]. This feature changes when we increase $g_{aa} = g$ to larger positive values, thereby promoting (anti-)flocking. Fig. 5 shows the corresponding MF stability diagram for the antagonistic case $g_{AB} = -g_{BA}$. Beyond the critical (flocking) line $g \approx 6$, the largest eigenvalue stays real only in the reciprocal limit (white line). In all other cases the largest eigenvalues become imaginary. Moreover, only in this regime ($g \gtrsim 6$), we find exceptional points (eigenvalue coalescence with parallel eigenvectors) that have been related to parity-time symmetry breaking of the dynamics in simpler NR systems [44–46]. A more detailed analysis of this phenomenon and its interplay with the density dynamics will be given in a future paper.

Conclusion.—The present study demonstrates how NR orientational couplings that do not directly affect the particle positions (contrary to, e.g., hydrodynamic or dipolar interactions), combined with active translational motion, leads to asymmetric density dynamics, that is, partial demixing. The behavior found here is in stark contrast to equilibrium mixtures where demixing rather results from (comparatively) small interspecies coupling strengths [5] or different particle shapes [2]. In active systems, demixing has been found before, but always caused

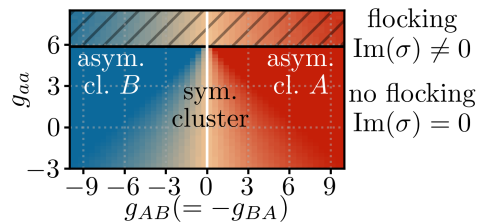


FIG. 5. Stability diagram in the plane spanned by $g_{AB} = \delta = -g_{BA}$ and $g_{aa} = g$. Colors correspond to phase separation angle α as used in Fig. 1 and 4.

by conservative interactions [26, 31] or parameters coupling to the translational dynamics such as diffusion constants [22] and active speed differences [19–21]. In our system, partial demixing is truly caused by NR orientational couplings and the fact that it involves *two* types of order parameters which have, so far, rather been considered separately: (conserved) density fields (as appearing in scalar NR systems) *and* (non-conserved) polarization fields (as appearing in flocking models). We note that the here observed dynamical asymmetry is *not* related to exceptional-point behavior and parity-time symmetry breaking that has been discussed before [44–46]. Exceptional points do occur, however, at larger polar coupling strength. Moreover, at very strong NR coupling, clustering disappears. Suppression of MIPS due to NR has been seen before [32], but with more complicated NR couplings between orientations and positions.

The present phenomenology is apparent already on the MF hydrodynamic level (with appropriately chosen particle velocity) and is supported by BD simulations, revealing remarkable consistency between the different levels of description (which is not clear *ad hoc* [61]). Still, BD simulations give important additional insights such as the polarization of the single-species cluster(s), structural aspects such as correlations and cluster sizes [55], and dynamical properties (“chase and run”-like behavior).

Our results could, in principle, be tested in mixtures of Quincke rollers [52] where, in addition, nonreciprocal hydrodynamic effects play a role [23]. Alternatively, the interactions could be engineered in robotic experiments [62]. The here presented dynamical behavior could also be relevant in the broader context of non-equilibrium liquid-liquid phase separation [1] of multicomponent biological organisms, or active self-assembling mechanisms [27, 63]. Future work should focus on the behavior at larger coupling strengths, as well as on thermodynamic implications [64–66]. Furthermore, it would be intriguing to have a classification of the present, mixed order-parameter model into wider classes of pattern-forming models, as it has been recently been done for the NR Cahn-Hilliard model [47].

This work was funded by the Deutsche Forschungsgemeinschaft (DFG, German Research Foundation) – Pro-

jektnummer 163436311 (SFB 910) and Projektnummer 517665044.

* k.kreienkamp@tu-berlin.de

† sabine.klapp@tu-berlin.de

- [1] J. S. Rowlinson and F. L. Swinton, *Liquids and liquid mixtures: Butterworths monographs in chemistry* (Butterworth-Heinemann, 2013).
- [2] M. Adams, Z. Dogic, S. L. Keller, and S. Fraden, Entropically driven microphase transitions in mixtures of colloidal rods and spheres, *Nature* **393**, 349 (1998).
- [3] S. Asakura and F. Oosawa, Interaction between particles suspended in solutions of macromolecules, *J. Polym. Sci.* **33**, 183 (1958).
- [4] T. Biben, P. Bladon, and D. Frenkel, Depletion effects in binary hard-sphere fluids, *J. Phys. Condens. Matter* **8**, 10799 (1996).
- [5] N. Wilding, F. Schmid, and P. Nielaba, Liquid-vapor phase behavior of a symmetrical binary fluid mixture, *Phys. Rev. E* **58**, 2201 (1998).
- [6] S. Elias and E. Banin, Multi-species biofilms: living with friendly neighbors, *FEMS Microbiol. Rev.* **36**, 990 (2012).
- [7] E. Ben-Jacob, A. Finkelshtein, G. Ariel, and C. Ingham, Multispecies swarms of social microorganisms as moving ecosystems, *Trends Microbiol.* **24**, 257 (2016).
- [8] S. Peled, S. D. Ryan, S. Heidenreich, M. Bär, G. Ariel, and A. Be'Er, Heterogeneous bacterial swarms with mixed lengths, *Phys. Rev. E* **103**, 032413 (2021).
- [9] K. C. Leptos, J. S. Guasto, J. P. Gollub, A. I. Pesci, and R. E. Goldstein, Dynamics of enhanced tracer diffusion in suspensions of swimming eukaryotic microorganisms, *Phys. Rev. Lett.* **103**, 198103 (2009).
- [10] J. Stenhammar, R. Wittkowski, D. Marenduzzo, and M. E. Cates, Activity-induced phase separation and self-assembly in mixtures of active and passive particles, *Phys. Rev. Lett.* **114**, 018301 (2015).
- [11] Y. G. Zhao and H. Zhang, Phase separation in membrane biology: the interplay between membrane-bound organelles and membraneless condensates, *Dev. Cell* **55**, 30 (2020).
- [12] P. Sens and M. S. Turner, Microphase separation in nonequilibrium biomembranes, *Phys. Rev. Lett.* **106**, 238101 (2011).
- [13] M. C. Marchetti, J.-F. Joanny, S. Ramaswamy, T. B. Liverpool, J. Prost, M. Rao, and R. A. Simha, Hydrodynamics of soft active matter, *Rev. Mod. Phys.* **85**, 1143 (2013).
- [14] T. Vicsek, A. Czirók, E. Ben-Jacob, I. Cohen, and O. Shochet, Novel type of phase transition in a system of self-driven particles, *Phys. Rev. Lett.* **75**, 1226 (1995).
- [15] G. Grégoire and H. Chaté, Onset of collective and cohesive motion, *Phys. Rev. Lett.* **92**, 025702 (2004).
- [16] M. E. Cates and J. Tailleur, Motility-induced phase separation, *Annu. Rev. Condens. Matter Phys.* **6**, 219 (2015).
- [17] J. Bialké, H. Löwen, and T. Speck, Microscopic theory for the phase separation of self-propelled repulsive disks, *EPL* **103**, 30008 (2013).
- [18] I. Buttinoni, J. Bialké, F. Kümmel, H. Löwen, C. Bechinger, and T. Speck, Dynamical clustering and phase separation in suspensions of self-propelled colloidal particles, *Phys. Rev. Lett.* **110**, 238301 (2013).
- [19] S. Adhikary and S. Santra, Pattern formation and phase transition in the collective dynamics of a binary mixture of polar self-propelled particles, *Phys. Rev. E* **105**, 064612 (2022).
- [20] T. Kolb and D. Klotsa, Active binary mixtures of fast and slow hard spheres, *Soft Matter* **16**, 1967 (2020).
- [21] E. Ilker and J.-F. Joanny, Phase separation and nucleation in mixtures of particles with different temperatures, *Phys. Rev. Res.* **2**, 023200 (2020).
- [22] S. N. Weber, C. A. Weber, and E. Frey, Binary mixtures of particles with different diffusivities demix, *Phys. Rev. Lett.* **116**, 058301 (2016).
- [23] S. Maity and A. Morin, Spontaneous demixing of binary colloidal flocks, *Phys. Rev. Lett.* **131**, 178304 (2023).
- [24] C. Scheibner, A. Souslov, D. Banerjee, P. Surówka, W. T. Irvine, and V. Vitelli, Odd elasticity, *Nat. Phys.* **16**, 475 (2020).
- [25] R. K. Gupta, R. Kant, H. Soni, A. Sood, and S. Ramaswamy, Active nonreciprocal attraction between motile particles in an elastic medium, *Phys. Rev. E* **105**, 064602 (2022).
- [26] J. Agudo-Canalejo and R. Golestanian, Active phase separation in mixtures of chemically interacting particles, *Phys. Rev. Lett.* **123**, 018101 (2019).
- [27] R. Soto and R. Golestanian, Self-assembly of catalytically active colloidal molecules: Tailoring activity through surface chemistry, *Phys. Rev. Lett.* **112**, 068301 (2014).
- [28] S. Saha, S. Ramaswamy, and R. Golestanian, Pairing, waltzing and scattering of chemotactic active colloids, *New J. Phys.* **21**, 063006 (2019).
- [29] G. Tucci, R. Golestanian, and S. Saha, Nonreciprocal collective dynamics in a mixture of phoretic Janus colloids, arXiv preprint arXiv:2402.09279 (2024).
- [30] J. P. Banerjee, R. Mandal, D. S. Banerjee, S. Thutupalli, and M. Rao, Unjamming and emergent nonreciprocity in active ploughing through a compressible viscoelastic fluid, *Nat. Commun.* **13**, 4533 (2022).
- [31] Y. Duan, J. Agudo-Canalejo, R. Golestanian, and B. Mahault, Dynamical pattern formation without self-attraction in quorum-sensing active matter: The interplay between nonreciprocity and motility, *Phys. Rev. Lett.* **131**, 148301 (2023).
- [32] M. Knežević, T. Welker, and H. Stark, Collective motion of active particles exhibiting non-reciprocal orientational interactions, *Sci. Rep.* **12**, 19437 (2022).
- [33] A. J. Lotka, Analytical note on certain rhythmic relations in organic systems, *Proc. Natl. Acad. Sci. U.S.A.* **6**, 410 (1920).
- [34] V. Volterra, Fluctuations in the abundance of a species considered mathematically, *Nature* **118**, 558 (1926).
- [35] C. H. Meredith, P. G. Moerman, J. Groenewold, Y.-J. Chiu, W. K. Kegel, A. van Blaaderen, and L. D. Zarzar, Predator-prey interactions between droplets driven by non-reciprocal oil exchange, *Nat. Chem.* **12**, 1136 (2020).
- [36] L. Barberis and F. Peruani, Large-scale patterns in a minimal cognitive flocking model: Incidental leaders, nematic patterns, and aggregates, *Phys. Rev. Lett.* **117**, 248001 (2016).
- [37] F. A. Lavergne, H. Wendehenne, T. Bäuerle, and C. Bechinger, Group formation and cohesion of active particles with visual perception-dependent motility, *Science* **364**, 70 (2019).
- [38] S. A. M. Loos, S. H. L. Klapp, and T. Martynek, Long-

- range order and directional defect propagation in the nonreciprocal XY model with vision cone interactions, *Phys. Rev. Lett.* **130**, 198301 (2023).
- [39] Y. Avni, M. Fruchart, D. Martin, D. Seara, and V. Vitelli, The non-reciprocal Ising model, arXiv preprint arXiv:2311.05471 (2023).
- [40] M. Fruchart, C. Scheibner, and V. Vitelli, Odd viscosity and odd elasticity, *Annu. Rev. Condens. Matter Phys.* **14**, 471 (2023).
- [41] A. Metelmann and A. A. Clerk, Nonreciprocal photon transmission and amplification via reservoir engineering, *Phys. Rev. X* **5**, 021025 (2015).
- [42] S. Zhang, Y. Hu, G. Lin, Y. Niu, K. Xia, J. Gong, and S. Gong, Thermal-motion-induced non-reciprocal quantum optical system, *Nat. Photonics* **12**, 744 (2018).
- [43] A. McDonald, R. Hanai, and A. A. Clerk, Nonequilibrium stationary states of quantum non-Hermitian lattice models, *Phys. Rev. B* **105**, 064302 (2022).
- [44] Z. You, A. Baskaran, and M. C. Marchetti, Nonreciprocity as a generic route to traveling states, *Proc. Natl. Acad. Sci. U.S.A.* **117**, 19767 (2020).
- [45] M. Fruchart, R. Hanai, P. B. Littlewood, and V. Vitelli, Non-reciprocal phase transitions, *Nature* **592**, 363 (2021).
- [46] S. Saha, J. Agudo-Canalejo, and R. Golestanian, Scalar active mixtures: The nonreciprocal Cahn-Hilliard model, *Phys. Rev. X* **10**, 041009 (2020).
- [47] T. Frohoff-Hülsmann and U. Thiele, Nonreciprocal Cahn-Hilliard model emerges as a universal amplitude equation, *Phys. Rev. Lett.* **131**, 107201 (2023).
- [48] T. Frohoff-Hülsmann, J. Wrembel, and U. Thiele, Suppression of coarsening and emergence of oscillatory behavior in a Cahn-Hilliard model with nonvariational coupling, *Phys. Rev. E* **103**, 042602 (2021).
- [49] R. Hanai, Nonreciprocal frustration: Time crystalline order-by-disorder phenomenon and a spin-glass-like state, *Phys. Rev. X* **14**, 011029 (2024).
- [50] R. Mandal, S. S. Jaramillo, and P. Sollich, Robustness of travelling states in generic non-reciprocal mixtures, arXiv preprint arXiv:2212.05618 (2022).
- [51] P. C. Hohenberg and B. I. Halperin, Theory of dynamic critical phenomena, *Rev. Mod. Phys.* **49**, 435 (1977).
- [52] A. Bricard, J.-B. Caussin, N. Desreumaux, O. Dauchot, and D. Bartolo, Emergence of macroscopic directed motion in populations of motile colloids, *Nature* **503**, 95 (2013).
- [53] K. L. Kreienkamp and S. H. L. Klapp, Clustering and flocking of repulsive chiral active particles with non-reciprocal couplings, *New J. Phys.* **24**, 123009 (2022).
- [54] M. Te Vrugt, J. Bickmann, and R. Wittkowski, How to derive a predictive field theory for active Brownian particles: a step-by-step tutorial, *J. Condens. Matter Phys.* **35**, 313001 (2023).
- [55] K. L. Kreienkamp and S. H. L. Klapp, Dynamical structures in phase-separating non-reciprocal polar active mixtures, accompanying manuscript submitted to *Phys. Rev. E* (2024).
- [56] Y.-J. Chiu and A. K. Omar, Phase coexistence implications of violating Newton's third law, *J. Chem. Phys.* **158** (2023).
- [57] X. S. Chen and F. Forstmann, The demixing and gas-liquid instability of a binary Yukawa fluid, *J. Chem. Phys.* **97**, 3696 (1992).
- [58] X. S. Chen and F. Forstmann, The phase instability of molecular fluid mixtures: dipolar and neutral hard spheres, *Mol. Phys.* **76**, 1203 (1992).
- [59] G. M. Range and S. H. L. Klapp, Pair formation and global ordering of strongly interacting ferrocolloid mixtures: An integral equation study, *J. Chem. Phys.* **124** (2006).
- [60] The same (real) (anti-)flocking instabilities are obtained when starting the analysis from a base state of homogeneous flocking. The asymmetric density dynamics can only be assessed when considering the disordered base state.
- [61] A. Dinelli, J. O'Byrne, A. Curatolo, Y. Zhao, P. Sollich, and J. Tailleur, Non-reciprocity across scales in active mixtures, *Nat. Commun.* **14**, 7035 (2023).
- [62] J. Chen, X. Lei, Y. Xiang, M. Duan, X. Peng, and H. Zhang, Emergent chirality and hyperuniformity in an active mixture with nonreciprocal interactions, *Phys. Rev. Lett.* **132**, 118301 (2024).
- [63] T. Yu, P. Chuphal, S. Thakur, S. Y. Reigh, D. P. Singh, and P. Fischer, Chemical micromotors self-assemble and self-propel by spontaneous symmetry breaking, *Chem. Commun.* **54**, 11933 (2018).
- [64] S. A. M. Loos and S. H. L. Klapp, Irreversibility, heat and information flows induced by non-reciprocal interactions, *New J. Phys.* **22**, 123051 (2020).
- [65] T. Suchanek, K. Kroy, and S. A. M. Loos, Irreversible mesoscale fluctuations herald the emergence of dynamical phases, *Phys. Rev. Lett.* **131**, 258302 (2023).
- [66] T. Suchanek, K. Kroy, and S. A. M. Loos, Time-reversal and parity-time symmetry breaking in non-Hermitian field theories, *Phys. Rev. E* **108**, 064123 (2023).

Supplemental Material to “Non-reciprocal alignment induces asymmetric clustering in active repulsive mixtures”

Kim L. Kreienkamp* and Sabine H. L. Klapp†
Institut für Theoretische Physik, Technische Universität Berlin

In this supplemental, we provide additional background on our models and methods of analysis. In particular, we introduce the microscopic Langevin equations as well as the associated continuum model that is used as the starting point of the linear stability analysis and characterization of instabilities on the mean-field level. Further, we define the pair correlation functions based on particle trajectories. Finally, we present the connection between the pair correlations and the structure factor matrix, which is used to quantify the degree of (a)symmetrical clustering.

CONTENTS

I. Microscopic model	1
II. Continuum model	2
A. Parameter choice with respect to particle-based model	3
III. Linear stability analysis	3
A. Stability matrix	3
B. Non-equilibrium phase characterization	4
C. Relation to exceptional points	5
IV. Pair correlation functions	6
V. Structure factor matrix	7
VI. List of supplementary videos	8
References	8

I. MICROSCOPIC MODEL

We consider a two-dimensional system of active particles comprising two species $a = A, B$. The binary mixture contains $N = N_A + N_B$ particles that are located at positions \mathbf{r}_α (with $\alpha = i_a = 1, \dots, N_a$) and move like active Brownian particles (ABP). They are subject to an additional torque due to orientational couplings. They self-propel with velocity v_0 in the direction $\mathbf{p}_\alpha(t) = (\cos \theta_\alpha, \sin \theta_\alpha)^T$, where θ_α is the polar angle. The overdamped Langevin equations (LE), governing the dynamics, are given by

$$\dot{\mathbf{r}}_\alpha(t) = v_0 \mathbf{p}_\alpha(t) + \mu_r \sum_{\beta \neq \alpha} \mathbf{F}_{\text{rep}}^\alpha(\mathbf{r}_\alpha, \mathbf{r}_\beta) + \boldsymbol{\xi}_\alpha(t) \quad (1a)$$

$$\dot{\theta}_\alpha(t) = \mu_\theta \sum_{\beta \neq \alpha} \mathcal{T}_{\text{al}}^\alpha(\mathbf{r}_\alpha, \mathbf{r}_\beta, \theta_\alpha, \theta_\beta) + \eta_\alpha(t), \quad (1b)$$

where the sums over particles $\beta = j_b = 1, \dots, N_b$ couple the dynamics of particle α to the position and orientation of all other particles of both species $b = A, B$.

The translational LE (1a) contains the repulsive force $\mathbf{F}_{\text{rep}}^\alpha = -\sum_{\beta \neq \alpha} \nabla_\alpha U(r_{\alpha\beta})$ between hard disks, derived from the Weeks-Chandler-Andersen (WCA) potential [1]

$$U(r_{\alpha\beta}) = \begin{cases} 4\epsilon \left[\left(\frac{\sigma}{r_{\alpha\beta}} \right)^{12} - \left(\frac{\sigma}{r_{\alpha\beta}} \right)^6 + \frac{1}{4} \right], & \text{if } r_{\alpha\beta} < r_c \\ 0, & \text{else} \end{cases}, \quad (2)$$

* k.kreienkamp@tu-berlin.de

† sabine.klapp@tu-berlin.de

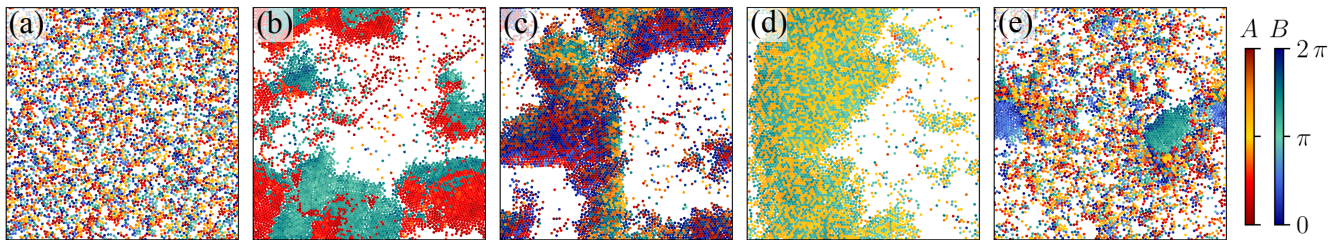


FIG. 1. Snapshots of Brownian dynamics simulations for (a) $g_{AB} = -g_{BA} = 20$ (disorder). (b) $g_{AB} = g_{BA} = -9$ (antiflocking). (c) $g_{AB} = g_{BA} = 1$ (MIPS). (d) $g_{AB} = g_{BA} = 9$ (flocking and phase separation). (e) $g_{AB} = -g_{BA} = -9$ (asymmetric clustering of species B). Other parameters are $g_{AA} = g_{BB} = 3$, $\text{Pe} = 40$, $\Phi = 0.4$.

where $r_{\alpha\beta} = |\mathbf{r}_{\alpha\beta}| = |\mathbf{r}_\alpha - \mathbf{r}_\beta|$. The characteristic energy scale of the potential is given by ϵ . The cut-off distance is $r_c = 2^{1/6} \sigma$. The particle diameter σ is taken as characteristic length scale, $\ell = \sigma$.

The rotational LE (1b) involves the torque given by

$$\mathcal{T}_{\text{al}}^\alpha(\mathbf{r}_\alpha, \mathbf{r}_\beta, \theta_\alpha, \theta_\beta) = k_{ab} \sin(\theta_\beta - \theta_\alpha) \Theta(R_\theta - r_{\alpha\beta}). \quad (3)$$

Here, k_{ab} denotes its strength and can be positive or negative. The step function with $\Theta(R_\theta - r_{\alpha\beta}) = 1$ if $r_{\alpha\beta} < R_\theta$ and zero otherwise, ensures that only particles within radius R_θ interact via the torque. Particles of species a tend to orient parallel (align) or antiparallel (antialign) with neighboring particles (within radius R_θ) of species b when $k_{ab} > 0$ or $k_{ab} < 0$, respectively. *Reciprocal* couplings are defined by the choice $k_{ab} = k_{ba}$. Then, particles of species a align (or antialign) with particles of species b in the same way as particles of species b with particles of species a . We specifically allow for *non-reciprocal* orientational couplings, for which $k_{ab} \neq k_{ba}$.

Both the position and orientation of the particles are subject to thermal noise, modeled as Gaussian white noise processes $\xi_\alpha(t)$ and $\eta_\alpha(t)$ of zero mean and variances $\langle \xi_{\alpha,k}(t) \xi_{\beta,l}(t') \rangle = 2\xi \delta_{\alpha\beta} \delta_{kl} \delta(t - t')$ and $\langle \eta_\alpha(t) \eta_\beta(t') \rangle = 2\eta \delta_{\alpha\beta} \delta(t - t')$, respectively. The (Brownian) time a (passive) particle needs to travel over its own distance is $\tau = \sigma^2/\xi$, which we take as characteristic time scale. The mobilities fulfill the Einstein relation and are connected to thermal noise via $\mu_r = \beta \xi$ and $\mu_\theta = \beta \eta$, where $\beta^{-1} = k_B T$ is the thermal energy with Boltzmann's constant k_B and temperature T .

To study the emerging dynamical structures in our system, we perform numerical Brownian Dynamics (BD) simulations of the LE (1). To this end, we introduce the following dimensionless parameters: the average area fractions $\Phi_a = \rho_0^a \pi \ell^2/4$ of species a with (number) density $\rho_0^a = N_a/L^2$, the reduced orientational coupling parameter $g_{ab} = k_{ab} \mu_\theta \tau$, and the Péclet number $\text{Pe} = v_0 \tau/\ell$, which quantifies the persistence of the motion of particles.

We perform particle simulations at a fixed combined average area fraction $\Phi = 0.4$, where $\Phi_A = \Phi_B = 0.2$, and Péclet number $\text{Pe} = 40$, while varying the orientational couplings strengths g_{ab} . We simulate $N = 5000$ particles, with equal particle numbers $N_A = N_B = 2500$ of both species, in a $L \times L$ box subjected to periodic boundary conditions. We use the particle diameter σ as characteristic length scale, $\ell = \sigma = 1$, and the time unit as $\tau = \sigma^2/\xi = 1$. The repulsive strength is chosen to be $\epsilon^* = \epsilon k_B T = 100$, where the thermal energy is set to be the energy unit ($k_B T = 1$). The diffusion constants are then given by $\xi = 1 \ell^2/\tau$ and $\eta = 3 \cdot 2^{-1/3}/\tau$. The cut-off distance for the torque is chosen to be $R_\theta = 2\ell$. The simulations are performed by initializing the system in a random configuration, integrating the equations of motions using an Euler-Mayurama algorithm, and letting the system evolve into its steady state before measuring quantities for phase characterization. To this end, we employ a timestep of $\Delta t = 10^{-5} \tau$ until the simulations have lasted for 120τ .

Snapshots of the Brownian dynamics simulations for different parameter combinations are shown in Fig. 1.

II. CONTINUUM MODEL

For the derivation of the continuum model associated to LE (1), we refer to [2, 3]. The final equations comprise the continuity equation for the densities $\rho^a(\mathbf{r}, t)$,

$$\partial_t \rho^a + \nabla \cdot \mathbf{j}_a = 0 \quad (4)$$

with flux

$$\mathbf{j}_a = v^{\text{eff}}(\rho) \mathbf{w}^a - D_t \nabla \rho^a. \quad (5)$$

parameter	definition	description
Pe	$v_0 \tau / \ell$	Péclet number
z	$\zeta \rho_0 \tau / \ell$	particle velocity-reduction
D_t	$\xi \tau / \ell^2$	translational diffusion
D_r	$\eta \tau$	rotational diffusion
g'_{ab}	$k_{ab} \mu_\theta R_\theta^2 \pi \rho_0^b \tau / 2$	orient. coupling strength

TABLE I. The five control parameters in the non-dimensionalized continuum equations (4) – (6) with characteristic time and length scales, τ and ℓ , and average density $\rho_0 = \sum_a \rho_0^a$.

The flux involves the polarization densities $\mathbf{w}^a(\mathbf{r}, t) = \rho^a \mathbf{P}^a$ with $\mathbf{P}^a(\mathbf{x}, t)$ being the polarization field, measuring the overall orientation of particles at a certain position. The polarization density \mathbf{w}^a evolves according to

$$\begin{aligned}
& \partial_t \mathbf{w}^a \\
&= -\frac{1}{2} \nabla (v^{\text{eff}}(\rho) \rho^a) - D_r \mathbf{w}^a + \sum_b g'_{ab} \rho^a \mathbf{w}^b + D_t \nabla^2 \mathbf{w}^a + \frac{v^{\text{eff}}(\rho)}{16 D_r} \nabla^2 (v^{\text{eff}}(\rho) \mathbf{w}^a) - \sum_{b,c} \frac{g'_{ab} g'_{ac}}{2 D_r} \mathbf{w}^a (\mathbf{w}^b \cdot \mathbf{w}^c) \\
& - \frac{z}{16 D_r} \nabla \rho \cdot [\nabla (v^{\text{eff}}(\rho) \mathbf{w}^a) - \nabla^* (v^{\text{eff}}(\rho) \mathbf{w}^{a*})] + \sum_b \frac{g'_{ab}}{8 D_r} [\mathbf{w}^b \cdot \nabla (v^{\text{eff}}(\rho) \mathbf{w}^a) + \mathbf{w}^{b*} \cdot \nabla (v^{\text{eff}}(\rho) \mathbf{w}^{a*}) \\
& - 2 \left\{ v^{\text{eff}}(\rho) \mathbf{w}^a \cdot \nabla \mathbf{w}^b + \mathbf{w}^b \nabla \cdot (v^{\text{eff}}(\rho) \mathbf{w}^a) - v^{\text{eff}}(\rho) \mathbf{w}^{a*} \cdot \nabla \mathbf{w}^{b*} - \mathbf{w}^{b*} \nabla \cdot (v^{\text{eff}}(\rho) \mathbf{w}^{a*}) \right\}].
\end{aligned} \tag{6}$$

The density flux \mathbf{j}_a given in Eq. (5) comprises that particles of species a move in space due to their self-propulsion in the direction \mathbf{w}^a . Importantly, the self-propulsion velocity is not constant but particles slow down in high-density regions. This is reflected in the density-dependent velocity $v^{\text{eff}}(\rho) = \text{Pe} - z \rho$ with $\rho = \sum_b \rho^b$. The flux further comprises translational diffusion. The evolution of the polarization density \mathbf{w}^a , given by Eq. (6), has various contributions: Particles tend to swim (with increasing speed) towards low-density regions (first term on right-hand side), the polarization decays due to rotational diffusion (second term), and orientations of all particles are coupled (third term). The remaining terms are diffusional and non-linear contributions, which smooth out low- and high-polarization regions.

In Eq. (6), we have introduced $\mathbf{w}^* = (w_y, -w_x)^T$ and $\nabla^* = (\partial_y, -\partial_x)^T$. We non-dimensionalized the equations with a characteristic time scale τ and a characteristic length scale ℓ . Further, particle and polarization densities of species a are scaled with the average particle density ρ_0^a . There are five remaining dimensionless control parameters. These are the Péclet number $\text{Pe} = v_0 \tau / \ell$, the velocity-reduction parameter $z = \zeta \rho_0 \tau / \ell$ due to the environment, the translational diffusion coefficient $D_t = \xi \tau / \ell^2$, the rotational diffusion coefficient $D_r = \eta \tau$, and the relative orientational coupling parameter $g'_{ab} = k_{ab} \mu_\theta R_\theta^2 \pi \rho_0^b \tau / 2$. The five control parameters are summarized in Table I.

A. Parameter choice with respect to particle-based model

In our continuum model, most parameters can be directly adopted from the considered particle simulation parameters. These include the Péclet number, $\text{Pe} = 40$, and the rotational diffusion constant, $D_r = \eta \tau = 3 \cdot 2^{-1/3}$. The area fraction in particle simulations, $\Phi = 0.4$, corresponds to the number density $\rho_0 = 2 \rho_0^a = 4 / \pi \Phi$, where $\rho_0^a = 2 / \pi \Phi$. The orientational couplings in continuum simulations (g'_{ab}) are related to those in the particle simulations (g_{ab}) via $g'_{ab} = 1.6 g_{ab}$, given $R_\theta = 2 \ell$. We consider a case with fixed weak intraspecies coupling strengths, $g_{AA} = g_{BB} = 3$, while the interspecies coupling strengths g_{AB} and g_{BA} are chosen independently. However, there are two parameters that require special attention: the velocity reduction parameter, ζ , and the translational diffusion constant, D_t . For details regarding the parameter choice, see [3]. We choose $D_t = 10$. Further, we obtain the non-dimensionalized velocity reduction parameter $z = \zeta \rho_0 \tau / \ell = 57.63 = 0.37 \text{Pe} / \rho_0^a$. This velocity reduction parameter places the system well within the MIPS instability region for a wider range of alignment strengths [2].

III. LINEAR STABILITY ANALYSIS

A. Stability matrix

We analytically determine the linear stability of the disordered, uniform state characterized by a uniform density and zero polarization for both species $a = A, B$, i.e., $(\rho_a, \mathbf{w}_a) = (\rho_0^a, \mathbf{0})$. To achieve this, we consider perturbations

of the disordered state involving all wave vectors \mathbf{k} , expressed as plane waves with a (complex) growth rate $\sigma(k)$ and amplitudes $\hat{\rho}^a(k)$ and $\hat{\mathbf{w}}^a(k)$ [3]. Since we investigate the stability of the isotropic disordered base state, the growth rate σ depends only on the wave number $k = |\mathbf{k}|$.

We are interested in perturbations in the combined field quantities $\rho^A + \rho^B$, $\rho^A - \rho^B$, $\mathbf{w}^A + \mathbf{w}^B$, and $\mathbf{w}^A - \mathbf{w}^B$. Starting from the continuum Eqs. (4) - (6), linearization with respect to the perturbation leads to an eigenvalue equation

$$\sigma(k) \mathbf{v}(k) = \mathcal{M}(k) \cdot \mathbf{v}(k) \quad (7)$$

for each k . The eigenvector $\mathbf{v}(k) = (\hat{\rho}^A + \hat{\rho}^B, \hat{\rho}^A - \hat{\rho}^B, \hat{w}_x^A + \hat{w}_x^B, \hat{w}_y^A + \hat{w}_y^B, \hat{w}_x^A - \hat{w}_x^B, \hat{w}_y^A - \hat{w}_y^B)^T$ contains the possible perturbations of the particle densities and the two components of the polarization densities. The 6×6 matrix $\mathcal{M}(k)$ is given by

$$\mathcal{M}(k) = \begin{pmatrix} -D_t k^2 & 0 & -i k_x v(\rho_0) & -i k_y v(\rho_0) & 0 & 0 \\ 0 & -D_t k^2 & 0 & 0 & -i k_x v(\rho_0) & -i k_y v(\rho_0) \\ -\frac{i}{2}(v(\rho_0) - z\rho_0)k_x & 0 & C_{++} - D_w & 0 & C_{+-} & 0 \\ -\frac{i}{2}(v(\rho_0) - z\rho_0)k_y & 0 & 0 & C_{++} - D_w & 0 & C_{+-} \\ 0 & -\frac{i}{2}v(\rho_0)k_x & C_{-+} & 0 & C_{--} - D_w & 0 \\ 0 & -\frac{i}{2}v(\rho_0)k_y & 0 & C_{-+} & 0 & C_{--} - D_w \end{pmatrix}, \quad (8)$$

where $\rho_0 = \rho_0^A + \rho_0^B$, $V = v(\rho_0) - z\rho_0^a$, $D_w = \mathcal{D}_a k^2 + D_r$, and $\mathcal{D}_a = v^2(\rho_0)/(16 D_r) + D_t$. The orientation couplings are given by

$$C_{++} = \frac{\rho_0^a}{2}(g'_{AA} + g'_{AB} + g'_{BA} + g'_{BB}), \quad (9)$$

$$C_{+-} = \frac{\rho_0^a}{2}(g'_{AA} - g'_{AB} + g'_{BA} - g'_{BB}), \quad (10)$$

$$C_{-+} = \frac{\rho_0^a}{2}(g'_{AA} + g'_{AB} - g'_{BA} - g'_{BB}), \quad (11)$$

$$C_{--} = \frac{\rho_0^a}{2}(g'_{AA} - g'_{AB} - g'_{BA} + g'_{BB}). \quad (12)$$

Solving the eigenvalue Eq. (7), we can analytically determine the (complex) growth rates $\sigma(k)$. The real part of the eigenvalues, $\text{Re}(\sigma)$, determines the actual growth or decay of the perturbations. Non-zero imaginary parts indicate oscillatory behavior. The disordered state is linearly stable when $\text{Re}(\sigma(k)) < 0$ for all k . On the other hand, the disordered state is linearly unstable if $\text{Re}(\sigma(k)) > 0$ for any k . We use the largest value of the six $\text{Re}(\sigma)$ and corresponding eigenvector to determine the type of emerging dynamics at short times [2].

B. Non-equilibrium phase characterization

We use the eigenvalues and the eigenvector corresponding to the largest eigenvalue to characterize the non-equilibrium phases emerging in our system. Details regarding the characterization can be found in [3].

The stability of the disordered (base) state is determined by the real parts of the (six) eigenvalues, $\text{Re}(\sigma_i)$. The disordered state is unstable as soon as any eigenvalue has a positive real part at any wave number k . We follow our earlier work [2] to analyze the largest real eigenvalues and corresponding eigenvector in order to determine the type of emerging dynamics at short times.

In case real parts of the eigenvalues are positive at zero wave number ($k = 0$), we can deduce that the instabilities concern the polarization dynamics, that is, (*anti-*)*flocking*. The reason is that the growth rate at $k = 0$ determines the growth or decay of spatially integrated fields. While the polarization field is not a conserved quantity, the particle density is. Hence, at $k = 0$ the density-associated growth rates must vanish and all instabilities must be related to polarization dynamics. The type of flocking (parallel or anti-parallel) is indicated by the eigenvector $\mathbf{v}(k = 0)$ corresponding to $\text{Re}(\sigma(k = 0)) > 0$. The largest entry of the eigenvector in $\hat{\mathbf{w}}^A + \hat{\mathbf{w}}^B$ predicts (parallel) flocking, while the largest entry in $\hat{\mathbf{w}}^A - \hat{\mathbf{w}}^B$ predicts (anti-parallel) anti-flocking.

The density dynamics corresponds to instabilities at finite wavenumbers ($k > 0$). Here, we consider only the two density-related entries of the (normalized) eigenvector, $\mathbf{v}_\rho = (\hat{\rho}^A + \hat{\rho}^B, \hat{\rho}^A - \hat{\rho}^B)^T$, at small $k > 0$. *Symmetric*

non-eq. phase	eigenvalues σ_i	eigenvector \mathbf{v} of largest real eigenvalue
disorder	$\text{Re}(\sigma_i(k)) \leq 0$ for all k and $i = 0, \dots, 6$	–
flocking	$\text{Re}(\sigma_i(k=0)) > 0$ for any i	largest entries of eigenvector in $\hat{\mathbf{w}}^A + \hat{\mathbf{w}}^B$
anti-flocking	$\text{Re}(\sigma_i(k=0)) > 0$ for any i	largest entries of eigenvector in $\hat{\mathbf{w}}^A - \hat{\mathbf{w}}^B$
sym. clustering	$\text{Re}(\sigma_i(k=0)) \leq 0$ for all i and global maximum $\text{Re}(\sigma_i(k_{\max}))$ at $k_{\max} > 0$ for any i	$\alpha \approx 0$
asym. cl. A	$\text{Re}(\sigma_i(k=0)) \leq 0$ for all i and global maximum $\text{Re}(\sigma_i(k_{\max}))$ at $k_{\max} > 0$ for any i	$0 < \alpha < \pi/2$
asym. cl. B	$\text{Re}(\sigma_i(k=0)) \leq 0$ for all i and global maximum $\text{Re}(\sigma_i(k_{\max}))$ at $k_{\max} > 0$ for any i	$-\pi/2 < \alpha < 0$

TABLE II. Characterization of non-equilibrium phases in the repulsive binary mixture with non-reciprocal orientational alignment couplings in terms of eigenvalues and eigenvector corresponding to largest eigenvalue. The angle $\alpha = \arccos(\mathbf{v}_\rho \cdot \mathbf{x}_{\text{con}})$ with $\mathbf{v}_\rho = (\hat{\rho}^A + \hat{\rho}^B, \hat{\rho}^A - \hat{\rho}^B)^\top$ and $\mathbf{x}_{\text{con}} = (1, 0)^\top$ indicates the type of phase separation. See also [3].

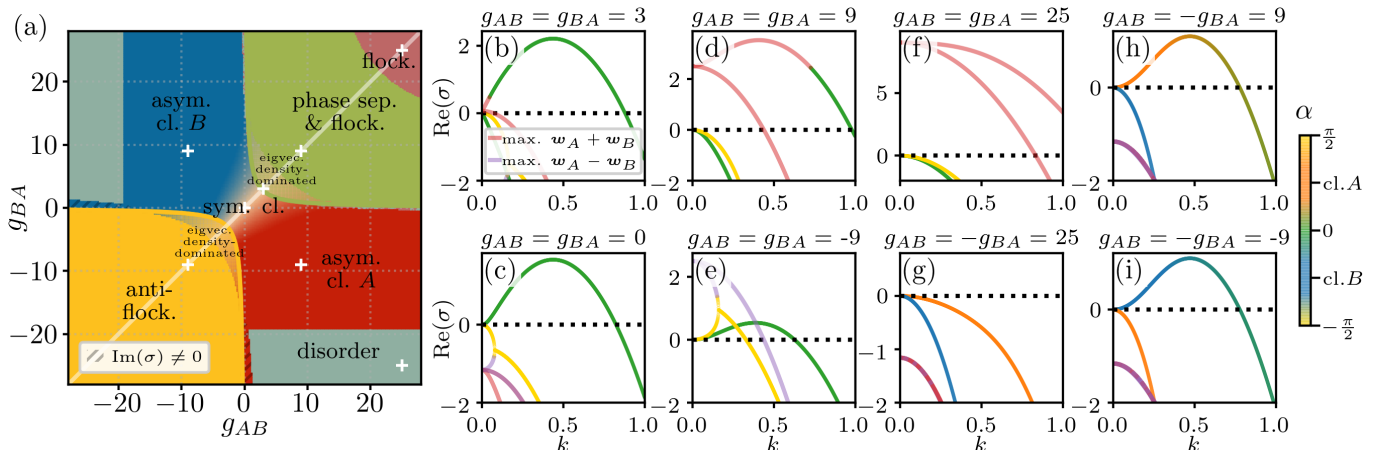


FIG. 2. Non-equilibrium phase diagram and respective growth rates. (a) Phase diagram. (b-g) Growth rate for various parameter combinations. The phases are determined from linear stability analyses of the disordered base state of the hydrodynamic Eqs. (4)-(6). The white crosses in (a) indicate the parameter combinations whose growth rates are plotted in (b-g). Additional parameters are set to $g_{AA} = g_{BB} = 3$, $\text{Pe} = 40$, $\Phi = 0.4$. See also [3].

clustering corresponds to $\mathbf{v}_\rho = \mathbf{x}_{\text{con}} = (1, 0)^\top$. The angle $\alpha = \arccos(\mathbf{v}_\rho \cdot \mathbf{x}_{\text{con}})$ between \mathbf{v}_ρ and \mathbf{x}_{con} is approximately 0. *Demixing* corresponds to \mathbf{v}_ρ close to $(0, 1)^\top$ with $\alpha \approx \pm\pi/2$. *Asymmetrical clustering* is quantified by intermediate angles α : For asymmetrical clusters of species A (B), the angle is $0 < \alpha < \pi/2$ ($-\pi/2 < \alpha < 0$).

The characterization is summarized in Table II and Fig. 2 shows exemplary real growth rates with indicated largest entries of eigenvectors. Note that (anti-)flocking and (a)symmetric clustering can either occur independent of each other or in combination.

In our system with relatively weak intraspecies alignment couplings of $g_{AA} = g_{BB} = 3$, the eigenvalues are real for a majority of intraspecies coupling strengths. For eigenvalues with positive real part and non-zero imaginary part, instabilities are oscillatory, indicating non-stationary emerging phases.

C. Relation to exceptional points

Exceptional transitions have been related to parity-time symmetry breaking transitions in non-reciprocal scalar [4, 5] and strongly coupled polar active systems [6]. In conserved scalar systems, exceptional points mark a transition from static patterns to traveling waves [4]. In polar systems, exceptional transitions separate regimes of (anti-)flocking in constant direction of polarization and chiral phases, where the polarization direction rotates in time [6]. Here, we briefly discuss the appearance of exceptional points in the present system.

By definition, exceptional points are points, where eigenvalues of the linear stability matrix coalesce and the eigenvectors become parallel [7]. In this study, we consider the isotropic disordered state (with constant density and vanishing polarization) as fixed point. The matrix (8) determines the linear stability of this disordered base state. In Fig. 3, we show the corresponding six eigenvalues σ at $k = 0$ as a function of g_{AB} . We choose $g_{BA} = -g_{AB} - d$

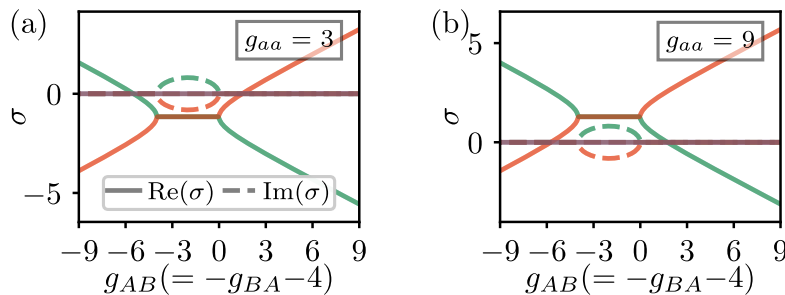


FIG. 3. Eigenvalues of isotropic disordered base state for $g_{AB} = g_{BA} - 4$ at $k = 0$ and (a) $g_{AA} = g_{BB} = 3$, (b) $g_{AA} = g_{BB} = 9$. At $g_{AB} = 0$ and $g_{AB} = -4$, four eigenvalues coalesce and form two complex conjugate pairs. The eigenvectors corresponding to the complex conjugate pairs become parallel. Below the flocking transition line (“weak intra-species couplings” with $g_{aa} = 3$), the real part of the eigenvalues, $\text{Re}(\sigma)$, is negative as long as $\text{Im}(\sigma) \neq 0$. For stronger intra-species couplings ($g_{aa} = 9$), the formation of complex conjugate pairs with parallel eigenvectors indicates exceptional points since $\text{Re}(\sigma) > 0$ as long as $\text{Im}(\sigma) \neq 0$.

with $d = 4$. Further, we set $g_{AA} = g_{BB} = g_{aa} = 3$ in Fig. 3(a) and $g_{aa} = 9$ in Fig. 3(b). The two eigenvalues, which correspond to density fluctuations, are zero at $k = 0$, regardless of g_{AB} (compare Sec. III B). The other four eigenvalues come in pairs (and overlap in Fig. 3) for the here considered cases.

Regardless of g_{aa} , we can make the following observation. For $g_{AB} < -d = -4$ and $g_{AB} > 0$, the two pairs of eigenvalues are distinct and real (with vanishing imaginary part). At $g_{AB} = 0$ and $g_{AB} = -4$, the four (non-zero) eigenvalues coalesce and form two complex conjugate pairs. Hence, for $-4 < g_{AB} < 0$, all non-zero eigenvalues are the same and have a non-zero imaginary part. The points of eigenvalue coalescence are $g_{AB} = 0, -4$. The eigenvectors corresponding to the complex conjugate pairs become parallel at these points.

Depending on g_{aa} , the points of eigenvalue coalescence have different implications. Below the flocking transition line [“weak intra-species couplings” with $g_{aa} = 3$, Fig. 3(a)], the real part of the eigenvalues, $\text{Re}(\sigma)$, is negative as long as $\text{Im}(\sigma) \neq 0$. For stronger intra-species couplings [$g_{aa} = 9$, Fig. 3(b)], the formation of complex conjugate pairs with parallel eigenvectors indicates exceptional points since $\text{Re}(\sigma) > 0$ as long as $\text{Im}(\sigma) \neq 0$. This means that the exceptional transition only results in instabilities for strong intra-species couplings. In particular, for our system and chosen parameters (see Sec. II A), the flocking transition line $g_{aa} \approx 6$ marks the strength of when exceptional transitions play a role in the stability of the disordered base state. For $g_{aa} \gtrsim 6$, flocking occurs for all g_{AB}, g_{BA} . The difference in dynamical behavior for g_{aa} below and above the exceptional transition line is shown in Fig. 5 in the main text.

The exceptional points of the disordered fixed points in the (non-repulsive) polar system considered in [6] match those found here. The transition happens for either $g_{AB} = 0$ or $g_{BA} = 0$, whereby the respective other inter-species coupling strength can be chosen arbitrarily. Additionally to the disordered base state, also a homogeneous (anti-)flocking state was considered in [6]. This makes sense in the regime of strong intra-species coupling strengths with $g_{aa} \gtrsim 6$. We will consider this regime in future research to gain insights into how non-reciprocal alignment effects the density dynamics in the presence of exceptional points.

IV. PAIR CORRELATION FUNCTIONS

Information on the translational structure in our active binary mixture are captured by the pair correlation function $G_{ab}(\mathbf{r})$, which describes the distribution of distance vectors \mathbf{r} between pairs of particles belonging to species a and b [8]. In homogeneous systems, we define $G_{ab}(\mathbf{r})$ as [8, 9]

$$G_{ab}(\mathbf{r}) = \frac{1}{\Omega} \sum_{a_i=1}^{N_a} \sum_{\substack{b_j=1 \\ (b_j \neq a_i)}}^{N_b} \langle \delta(\mathbf{r} - (\mathbf{r}_{a_i} - \mathbf{r}_{b_j})) \rangle, \quad (13)$$

where $\Omega = N_a N_b / V$ is the normalization and $V = L^2$ represents the volume of the system. $G_{ab}(\mathbf{r})$ tends to unity for $r \rightarrow \infty$ and vanishes for $r \rightarrow 0$ due to steric repulsion between particles.

Numerically, we determine $G_{ab}(r, \phi)$ by counting the particles found in small area fractions of distance $r + \Delta r$ and angle $\phi + \Delta\phi$ from the reference particle, such that we additionally normalize with the area fraction element

$\Delta A = r \Delta r \Delta \phi$, leading to

$$G_{ab}(r, \phi) = \frac{1}{\Omega_n} \sum_{a_i=1}^{N_a} \sum_{\substack{b_j=1 \\ (b_j \neq a_i)}}^{N_b} \left\langle \delta(r_{ij}^{ab} - r) \delta(\phi_{ij}^{ab} - \phi) \right\rangle \quad (14)$$

with $\Omega_n = N_a N_b \Delta A / V$. The relative particle position and angle are calculated as $r_{ij}^{ab} = |\mathbf{r}_{b_j} - \mathbf{r}_{a_i}|$ and $\phi_{ij}^{ab} = \angle(\mathbf{r}_{b_j} - \mathbf{r}_{a_i}, \mathbf{p}_{a_i})$.

Note that by construction, the pair distribution function is symmetric in the sense that $G_{AB} = G_{BA}$. The effect of non-reciprocity is expected to manifest itself in differences between the single-species correlations, such that $G_{AA} \neq G_{BB}$ [8]. We here focus on the radial correlations $G_{ab}(r) = \langle G_{ab}(r, \phi) \rangle_\phi$, given as the average over all relative angles ϕ . Details and further examples of pair correlation functions are shown in [3].

V. STRUCTURE FACTOR MATRIX

To characterize the density fluctuations close to phase transitions in our binary mixture, we took inspiration from established procedures applied in equilibrium mixtures [10, 11]. Our approach involves the computation of density fluctuation correlations of form $\langle \delta \rho_a(\mathbf{r}) \delta \rho_b(\mathbf{r}') \rangle$, where $a, b = A, B$. Here, we only consider instantaneous fluctuations and neglect all time-dependencies. The density fluctuation is given by $\delta \rho_a(\mathbf{r}) = \rho_a(\mathbf{r}) - \rho_0^a$ with ρ_0^a as the density of the homogeneous system. In an additionally isotropic system, the density fluctuations in Fourier space (denoted by a hat, $\hat{\cdot}$ [12]) reads [3]

$$\frac{1}{V} \langle \delta \hat{\rho}_a(\mathbf{k}) \delta \hat{\rho}_b(-\mathbf{k}) \rangle = \rho_0^a \rho_0^b \hat{h}_{ab}(k) + \delta_{ab} \rho_0^a, \quad (15)$$

where $h_{ab}(|\mathbf{r} - \mathbf{r}'|) = G_{ab}(|\mathbf{r} - \mathbf{r}'|) - 1$ denotes the total correlation function [9]. We note already here that in the present system, the assumption of homogeneity and isotropy holds only for short times (after starting from a random configuration).

To characterize the type of phase transition within the binary mixture, we consider two different types of fluctuations: fluctuations in the total density $\delta \hat{\rho}(k) = \delta \hat{\rho}_A(k) + \delta \hat{\rho}_B(k)$ and fluctuations in the concentration $\delta \hat{c}(k) = \delta \hat{\rho}_A(k) - \delta \hat{\rho}_B(k)$. These fluctuations can be written in terms of the structure factor matrix $\mathcal{S}(k)$, given by

$$\mathcal{S}(k) = \begin{pmatrix} S_{\rho\rho}(k) & S_{c\rho}(k) \\ S_{c\rho}(k) & S_{cc}(k) \end{pmatrix} \quad (16)$$

with matrix elements

$$\begin{aligned} S_{\rho\rho}(k) &= \frac{1}{V} \langle \delta \hat{\rho}(\mathbf{k}) \delta \hat{\rho}(-\mathbf{k}) \rangle \\ &= (\rho_0^A)^2 \hat{h}_{AA}(k) + (\rho_0^B)^2 \hat{h}_{BB}(k) + \rho_0^A + \rho_0^B + 2 \rho_0^A \rho_0^B \hat{h}_{AB}(k), \end{aligned} \quad (17)$$

$$\begin{aligned} S_{cc}(k) &= \frac{1}{V} \langle \delta \hat{c}(\mathbf{k}) \delta \hat{c}(-\mathbf{k}) \rangle \\ &= (\rho_0^A)^2 \hat{h}_{AA}(k) + (\rho_0^B)^2 \hat{h}_{BB}(k) + \rho_0^A + \rho_0^B - 2 \rho_0^A \rho_0^B \hat{h}_{AB}(k), \end{aligned} \quad (18)$$

and

$$\begin{aligned} S_{c\rho}(k) &= S_{\rho c}(k) = \frac{1}{V} \langle \delta \hat{c}(\mathbf{k}) \delta \hat{\rho}(-\mathbf{k}) \rangle \\ &= (\rho_0^A)^2 \hat{h}_{AA}(k) - (\rho_0^B)^2 \hat{h}_{BB}(k) + \rho_0^A - \rho_0^B. \end{aligned} \quad (19)$$

We assume that, as in equilibrium, an instability related to a phase transition is signaled by the divergence of fluctuations, i.e., one diverging eigenvalue $\lambda_{1/2}(k)$ of $\mathcal{S}(k)$. In particular, symmetric clustering (condensation) is characterized by diverging fluctuations in the total density and a demixing phase transition by diverging fluctuations in the concentration. Consequently, the eigenvalues $\lambda_{1/2}(k)$ and corresponding (normalized) eigenvectors $\mathbf{v}_{1/2}(k) = (\delta \hat{\rho}(k), \delta \hat{c}(k))^T$ of matrix $\mathcal{S}(k)$ indicate whether and what type of phase transition occurs. More specifically, when $\lambda_1^{-1}(k)$ or $\lambda_2^{-1}(k)$ goes to zero, the respective eigenvector \mathbf{v}_{\max} indicates whether the phase transition is predominantly

symmetric clustering ($\mathbf{v}_{\max} \approx \mathbf{x}_{\text{con}} = (1, 0)^T$) or de-mixing ($\mathbf{v}_{\max} \approx \mathbf{x}_{\text{dem}} = (0, 1)^T$). We quantify the degree of symmetric clustering and/or demixing in terms of the angle $\alpha = \arccos(\mathbf{v}_{\max} \cdot \mathbf{x}_{\text{con}})$ between the eigenvector \mathbf{v}_{\max} and the vector \mathbf{x}_{con} , representing symmetric clustering.

Besides symmetric clustering ($\alpha = 0$) and demixing ($\alpha = \pi/2$), the angle α also indicates whether rather species A or B forms clusters. In particular, $0 < \alpha < \pi/2$ corresponds to asymmetric clustering of species A and $-\pi/2 < \alpha < 0$ corresponds to asymmetric clustering of species B .

In our analysis, it turns out that the limit $k \rightarrow 0$ is the most relevant since $\lambda_{1/2}^{-1}$ are smallest there. Therefore, the presented results refer exclusively to this limit.

VI. LIST OF SUPPLEMENTARY VIDEOS

To visualize the dynamics of non-equilibrium phases exhibited in the binary mixture, we present videos of our BD simulations. They represent one exemplary non-equilibrium steady state for a single random initial configuration, respectively. The videos show

- the (reciprocal) flocking state for $g_{AB} = g_{BA} = 9$,
- the (reciprocal) anti-flocking state for $g_{AB} = g_{BA} = -9$,
- the (reciprocal) symmetric clustering state for $g_{AB} = g_{BA} = 1$,
- the (non-reciprocal) asymmetric B -clustering state for $g_{AB} = -g_{BA} = -9$,
- the (non-reciprocal) asymmetric A -clustering state for $g_{AB} = 6, g_{BA} = -9$,
- the (non-reciprocal) disordered for $g_{AB} = -g_{BA} = 25$.

The intraspecies couplings are set to $g_{AA} = g_{BB} = 3$. Other parameters are chosen as described in the Sec. I.

-
- [1] J. D. Weeks, D. Chandler, and H. C. Andersen, Role of repulsive forces in determining the equilibrium structure of simple liquids, *J. Chem. Phys.* **54**, 5237 (1971).
- [2] K. L. Kreienkamp and S. H. Klapp, Clustering and flocking of repulsive chiral active particles with non-reciprocal couplings, *New J. Phys.* **24**, 123009 (2022).
- [3] K. L. Kreienkamp and S. H. L. Klapp, Dynamical structures in phase-separating non-reciprocal polar active mixtures, accompanying manuscript submitted to *Phys. Rev. E* (2024).
- [4] Z. You, A. Baskaran, and M. C. Marchetti, Nonreciprocity as a generic route to traveling states, *Proc. Natl. Acad. Sci. U.S.A.* **117**, 19767 (2020).
- [5] S. Saha, J. Agudo-Canalejo, and R. Golestanian, Scalar active mixtures: The nonreciprocal Cahn-Hilliard model, *Phys. Rev. X* **10**, 041009 (2020).
- [6] M. Fruchart, R. Hanai, P. B. Littlewood, and V. Vitelli, Non-reciprocal phase transitions, *Nature* **592**, 363 (2021).
- [7] R. El-Ganainy, K. G. Makris, M. Khajavikhan, Z. H. Musslimani, S. Rotter, and D. N. Christodoulides, Non-Hermitian physics and PT symmetry, *Nature Physics* **14**, 11 (2018).
- [8] J. Bartnick, M. Heinen, A. V. Ivlev, and H. Löwen, Structural correlations in diffusiophoretic colloidal mixtures with nonreciprocal interactions, *J. Condens. Matter Phys.* **28**, 025102 (2015).
- [9] J.-P. Hansen and I. R. McDonald, *Theory of simple liquids: with applications to soft matter* (Academic press, 2013).
- [10] X. Chen and F. Forstmann, The demixing and gas-liquid instability of a binary Yukawa fluid, *J. Chem. Phys.* **97**, 3696 (1992).
- [11] X. Chen and F. Forstmann, The phase instability of molecular fluid mixtures: dipolar and neutral hard spheres, *Molecular Physics* **76**, 1203 (1992).
- [12] We define the (two-dimensional) Fourier transform as $\hat{f}(\mathbf{k}) = \int_{\mathbb{R}^2} f(\mathbf{r}) e^{-2\pi \mathbf{r} \cdot \mathbf{k}} d\mathbf{r}$ (with inverse $f(\mathbf{r}) = \int_{\mathbb{R}^2} \hat{f}(\mathbf{k}) e^{2\pi \mathbf{r} \cdot \mathbf{k}} d\mathbf{k}$). For a radially symmetric integral kernel, the two-dimensional Fourier transform is a Hankel or Fourier-Bessel transform (of order zero) with $\hat{f}(k) = 2\pi \int_0^\infty f(r) J_0(2\pi k r) r dr$, where $J_0(z)$ is the zeroth order Bessel function of the first kind.